Solid State Communications 193 (2014) 45–50

Contents lists available at ScienceDirect

Solid State Communications

journal homepage: www.elsevier.com/locate/ssc

Unusual correlation physics in a BCS superconductor, ZrB_{12}

Sangeeta Thakur, Kalobaran Maiti *

Department of Condensed Matter Physics and Materials' Science, Tata Institute of Fundamental Research, Homi Bhabha Road, Colaba, Mumbai 400005, India

ARTICLE INFO

Article history:
Received 19 May 2014
Accepted 28 May 2014
by S. Das Sarma
Available online 9 June 2014

Keywords:
A. Superconductor
D. Electronic structure
D. Electron correlation

ABSTRACT

We investigate the electronic structure of a conventional superconductor, ZrB_{12}, employing multiband Hubbard model and configuration interaction calculations. The calculated spectral functions within the cluster approximation provide a remarkable representation of *both* 3*d* and 3*p* spectra of Zr^{2+} species for the same set of electron–electron interaction parameters. Despite ZrB_{12} being a 4*d* transition metal based conventional superconductor, the electron correlation strength is found to be large. Ironically, the charge transfer energy is found to be smaller than the correlation strength placing this material in the charge transfer regime in the Zaanen–Swatzky–Allen phase diagram, which is unusual for early transition metal based systems.

1. Introduction

Conventional superconductors are the materials, where the conduction electrons form electron pairs (Cooper pairs) due to the electron–phonon coupling and the superconductivity is well captured by the Bardeen–Cooper–Schriefer (BCS) theory. The materials, where the superconductivity cannot be derived by the BCS theory, are termed as *unconventional superconductors* – in these systems, the electron–electron Coulomb repulsion plays significant role in their ground state properties. While most attentions have been paid towards understanding the anomalous behaviors in both superconducting and non-superconducting phases of the unconventional superconductors, it is found that conventional superconductors also exhibit unusual behaviors. For example, a 4*d* transition metal based dodecaboride superconductor, ZrB_{12}, is known to be a conventional superconductor. This material has been in the discussion for a long time due to the conflicts involving the nature of the superconducting transition [1–3], the mechanism of the transition from type I to type II/I superconductivity [3], whether it is a single gap [4] or two gap superconductor [5], *etc*.

In parallel to the oxide physics, these borides have been drawing much attention during past few decades followed by the findings of varied interesting properties in various forms of borides such as hexaborides, *M* B_6 and dodecaborides, *M* B_{12} (*M*=metals) [6–8]. These materials form cubic structures based on oversized crystalline cages of covalent boron ions. The metal atoms are enclosed within the cubic void spaces significantly larger than its ionic volume providing a large room for their dynamics. In particular, dodecaborides are known for their high melting point and hardness due to the B_{12} cuboctahedra forming a rigid, largely covalent bonded assembly with cubic symmetry. Two electron deficiency of the B_{12} units is balanced by the charge transfer from metal atoms. So, the dodecaborides containing metal atoms having more than two valence electrons are metallic [7]. ZrB_{12} is one such compound exhibiting highest superconducting critical temperature ($T_c \sim 6$ K) in *M* B_{12} family [8] and a model system to study the electron–phonon interaction induced effects in its superconductivity. Recent photoemission studies [9] exhibit multiple valence states and satellites in the core level spectra, which is the properties of correlated electron systems. In addition, signature of pseudogap above the superconducting transition temperature has also been observed in this system, which is unusual for a conventional superconductor [10]. ZrB_{12} is not the only compound that shows anomaly. The other compounds in the same *M* B_{12} family, YbB_{12}, UB_{12} and ReB_{12}, also exhibit unusual properties such as mixed valency, heavy fermion behavior, *etc*. All these results manifest the complexity of the electronic properties albeit simplicity in certain behavior.

In an uncorrelated system, the electronic structure can be captured reasonably well by the single particle descriptions. However, the final states of the photoemission spectra of a correlated system cannot be captured using single particle descriptions due to the interaction among the valence electrons as well as their interaction with the photo-holes. Since photoemission is a fast process, it has been found that cluster approximation often provides a good description of the photoemission spectra. There are many reports on the electronic structure calculations of 3*d* transition metal compounds [11–15] prompted by various exotic properties exhibited by these systems and the necessity of the model calculations due to strong electron correlation induced effects. Within these models, the electronic structure

* Corresponding author.
E-mail address: kbmaiti@tifr.res.in (K. Maiti).

http://dx.doi.org/10.1016/j.ssc.2014.05.027
0038-1098/

is derived in terms of a few parameters, namely the on-site Coulomb repulsion energy among the d electrons, U_{dd}, the charge transfer energy (Δ = the energy required to transfer an electron from the ligand levels to the d band), and the ligand p to metal d hybridization energy, T. These parameters for the 3d transition metal systems have been found to display systematic trends with formal valence state and atomic number, which has been summarized in a modified Zaanen–Swatzky–Allen (ZSA) phase diagram [16,17]. Within this description, the late 3d transition metal compounds are defined to be the charge transfer type system with $\Delta < U_{dd}$. The early 3d transition metal oxides show Mott–Hubbard type behavior possessing $U_{dd} < \Delta$. 4d systems are expected to be less correlated due to larger radial extension of the 4d orbitals relative to that in the 3d-systems suggesting a more pronounced Mott–Hubbard type behavior for such systems. However, recent studies indicated signature of significant electron correlation in 4d and 5d systems [18–20]. In order to address the complex electronic properties of these systems, we simulated the core level photoemission spectra of ZrB_{12} in this study within the cluster model. Our results exhibit evidence of the correlation physics in this material and the behavior is anomalous to the observations in 3d transition metal oxides.

2. Calculational details

Zr 3d and 3p photoemission spectra collected using Al $K\alpha$ radiations are adapted from Ref. [9] and shown in Fig. 1(a) and (b). Distinct contributions from multiple Zr species are evident in the experimental spectra. It was found that Zr^{1+} primarily appears in the surface spectra and Zr^0 contributes both in the bulk and in the surface electronic structures. The photoemission signal corresponding to the bulk electronic structure is primarily contributed by the Zr^{2+} species; these spectra are accompanied by satellite features in both 3d and 3p signals suggesting necessity of correlation physics for this system.

In order to model this system, we first investigate the crystal structure of ZrB_{12}. ZrB_{12} forms the cubic structure as shown in Fig. 1(c) with the space group $Fm3m$ and the lattice constant, a = 7.4075 Å. In this structure, Zr atoms are surrounded by B_{12} units arranged in an octahedral geometry as shown in the figure [21–23]. For better clarity, compressed B_{12} units are shown in Fig. 1 (d) demonstrating the scenario. Thus, one can form a cluster of Zr $(B_{12})_6$ similar to the cases of M O_6 octahedra in various 3d transition metal oxides. Here, we consider the whole B_{12} unit as a ligand and the corresponding electronic states are represented by the ligand p-states in the model. The excitation spectra in this process can now be described by the electronic interaction parameters for this cluster.

The model Hamiltonian is given by

$$H = \sum_i \epsilon_p n_{ip} + \sum_{\mu\sigma} (\epsilon_d - U_{dc} n_c) n_{\mu\sigma} + \sum_{i\mu\sigma} (t_{pd}^{i\mu} d_{\mu\sigma}^{\dagger} p_{i\sigma} + h.c.) + \frac{1}{2} U_{dd} N_d (N_d - 1) - J/2 \{ N_{d\uparrow}(N_{d\uparrow} - 1) + N_{d\downarrow}(N_{d\downarrow} - 1) \}$$

where $N_d = \sum_{\mu,\sigma} n_{\mu\sigma}$ and $N_{d\sigma} = \sum_{\mu} n_{\mu\sigma}$.

ϵ_d and ϵ_p are the bare energies of Zr 4d and ligand p orbitals, respectively. The indices i, μ and σ are used for ligand p states, Zr 4d states and their corresponding spins, respectively. The fermion

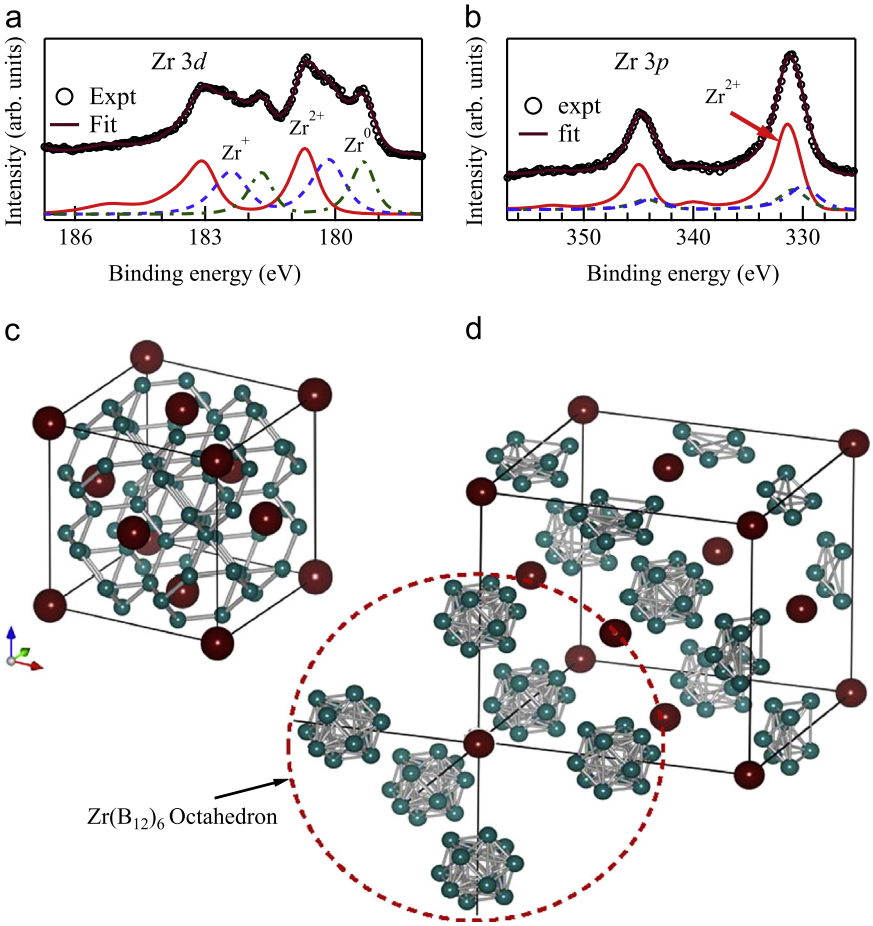

Fig. 1. Experimental (a) Zr 3d and (b) 3p core level spectra adapted from Ref. [9]. Experimental spectra show signature of Zr^0, Zr^{1+} and Zr^{2+} contributions represented by lines. (c) Crystal structure of ZrB_{12}. (d) The same structure is shown by compressing B_{12} units for clarity. The big circle encloses $Zr(B_{12})_6$ cluster.

operator $d^{\dagger}_{\mu\sigma}$ represents the creation of an electron in the d level and $p_{i\sigma}$ is the annihilation operator for the p level. U_{dc} is the on-site Coulomb interaction strength between the Zr 3d core hole and 4d electrons, and U_{dd} represents the Coulomb interaction strength among Zr 4d electrons. $t^{i\mu}_{pd}$ is the hopping interaction strength between Zr 4d and ligand p orbitals, and is expressed in terms of the Slater–Koster parameters: $pd\sigma$ and $pd\pi$ [24]. J is the exchange interaction strength. N_d is the total number of Zr 4d electrons.

The bare energy difference between the d and p orbitals ϵ_d–ϵ_p is represented by the charge transfer energy, Δ. Zr^{2+} corresponds to the electronic configuration $5s^2 4d^2$; the corresponding electronic state is expressed as $|d^2\rangle$. In this representation, the electronic configuration, $|d^3L\rangle$ represents a charge transferred state where an electron from the ligand bands has transferred to the d level making it d^3 and creating a ligand hole, L. Thus, the charge transfer energy, Δ, can be expressed as

$$\Delta = \epsilon(d^3L) - \epsilon(d^2) = \epsilon_d - \epsilon_p + 2U_{dd} - 2J + Q$$

Here, $Q = q1 - q2$, $q1$ is the crystal field splitting in the Zr 4d states and $q2$ is that in the ligand p derived $t_{2g} - e_g$ splitting. In our calculation we have kept Q=0 as the calculated results are not sensitive to the exact value of Q. In the presence of core hole, the Δ in the final state is given by

$$\Delta' = \Delta - U_{dc}$$

We have included configurations $|d^2\rangle$, $|d^3L^1\rangle$, $|d^4L^2\rangle$, $|d^5L^3\rangle$ and $|d^6L^4\rangle$ – the higher order terms have negligible contribution in the spectral functions. Basis states and the Hamiltonian matrix elements for $|d^2\rangle$, $|d^3L^1\rangle$, $|d^4L^2\rangle$, $|d^5L^3\rangle$ and $|d^6L^4\rangle$ configurations are given in the Supplementary materials.

3. Results

The experimental Zr 3d spectrum corresponding to Zr^{2+} species exhibits distinct signature of the main peak and satellites with an energy separation of 3 eV and the satellite to the main peak intensity ratio is found to be 0.68. The exchange interaction strength, J=0.7 eV, has been obtained from earlier report for 4d transition metal compounds [25]. We have varied U_{dd}, Δ and $pd\sigma$ to simulate the spectrum. It has been found that $pd\sigma = 0.6$ eV and $(pd\sigma)/(pd\pi) = 2.2$ provide the best description of the experimental spectrum. The magnitude of U_{dd} as a function of Δ is shown in Fig. 2(a) ($U_{dc}/U_{dd} \sim 0.98$–1.02). Calculations with various parameter sets show that U_{dd} increases with the increase in Δ. Interestingly, U_{dd} is always found to be larger than Δ placing this material in the charge transfer regime. This is significantly different from the scenario in 3d transition metal oxides – the early 3d transition metal compounds are primarily found in the Mott–Hubbard regime with U_{dd} smaller than Δ. Despite such large values of U_{dd} and Δ, total energy bandwidth, W of about 8 eV (obtained from the band structure calculations) makes this system metallic (pd-metal) [16,17].

From the ground state wavefunction, we calculated the 4d occupancy n_d as a function of U_{dd} and Δ; the results are shown in Fig. 2(a) as a function of Δ. n_d is found to decrease with the increase in Δ. The average value of n_d is close to 2.12, which indicates that ZrB_{12} is a mixed valent compound. This finding is in good agreement with the experimental results [9].

From Fig. 2(a), it is clear that the average value of U_{dd} and Δ is close to 4 eV and 3.4 eV, respectively. The corresponding calculated spectrum is shown by bar diagram in Fig. 2(b). In order to simulate the experimental results, the calculated spectrum is broadened by a Lorentzian broadening with energy-dependent full width at half maximum (FWHM, $\Gamma = a + b \times (BE)^{\alpha}$; a=0.1, b=0.05 and α=1) and a Gaussian representing experimental resolution broadening (FWHM=0.5 eV). The spin–orbit splitting (~2.4 eV) is set to the finding from the experimental spectrum. The final calculated spectrum is shown by solid line in Fig. 2 (b) exhibiting remarkably good representation of the experimental spectrum.

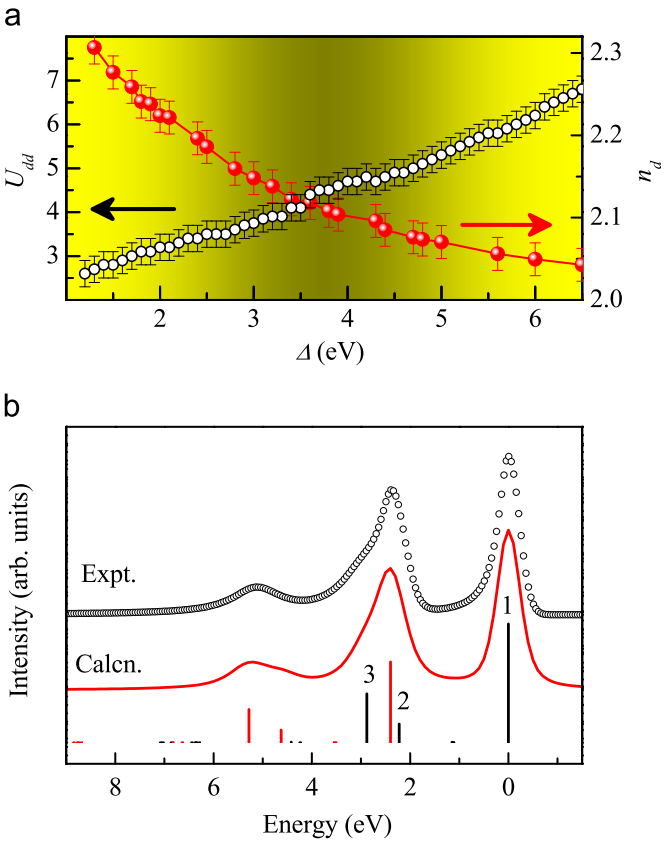

Fig. 2. (a) Calculated U_{dd} and n_d as a function of Δ those simulate the experimental 3d spectrum of Zr^{2+}. (b) Experimental spectrum (circles) is compared with the calculated result (bar diagram) corresponding to U_{dd}=4 eV and Δ=3.4 eV. The solid line represents the calculated spectra convoluted with the resolution broadening and life time broadening.

The eigenstate corresponding to the ground state possesses 88.0%, 11.75%, 0.24%, 1.55×10^{-3}%, and 3.79×10^{-6}% of $|d^2\rangle$, $|d^3L^1\rangle$, $|d^4L^2\rangle$, $|d^5L^3\rangle$ and $|d^6L^4\rangle$ configurations, respectively, leading to an n_d count of 2.12. In the calculated spectrum, in addition to the main peak denoted by '1' in the figure, we observe two intense satellite features appearing around 2.2 eV and 2.9 eV away from the main peak as marked by '2' and '3' in the figure for $3d_{5/2}$ photoemission signal. The final state corresponding to the main peak, '1', possesses about 30.51%, 39.51%, 26.21%, 2.45%, 1.29% and the most intense satellite peak, '3', possesses 54.88%, 4.31%, 34.59%, 4.29%, 1.91% of $|d^2\rangle$, $|d^3L^1\rangle$, $|d^4L^2\rangle$, $|d^5L^3\rangle$, $|d^6L^4\rangle$ configurations, respectively. This suggests that the main peak is primarily contributed by the well-screened feature, $|d^3L^1\rangle$ along with a sizable contribution from poorly screened, $|d^2\rangle$ and overscreened, $|d^4L^2\rangle$ states. The satellite peak, 3, is dominated by the poorly screened state, $|d^2\rangle$ along with a significant contribution from the overscreened $|d^4L^2\rangle$ feature. The satellite peak, 2, has dominant contribution (~73.62%) from the overscreened state, $|d^4L^2\rangle$ and relatively weaker contribution from the poorly screened state, $|d^2\rangle$ (~16.29%).

In order to establish the reliability of the estimated parameter values, we show the calculated results for the variation of U_{dd}, Δ, $pd\sigma$ and $pd\sigma/pd\pi$ in Fig. 3. In every case, one parameter is varied

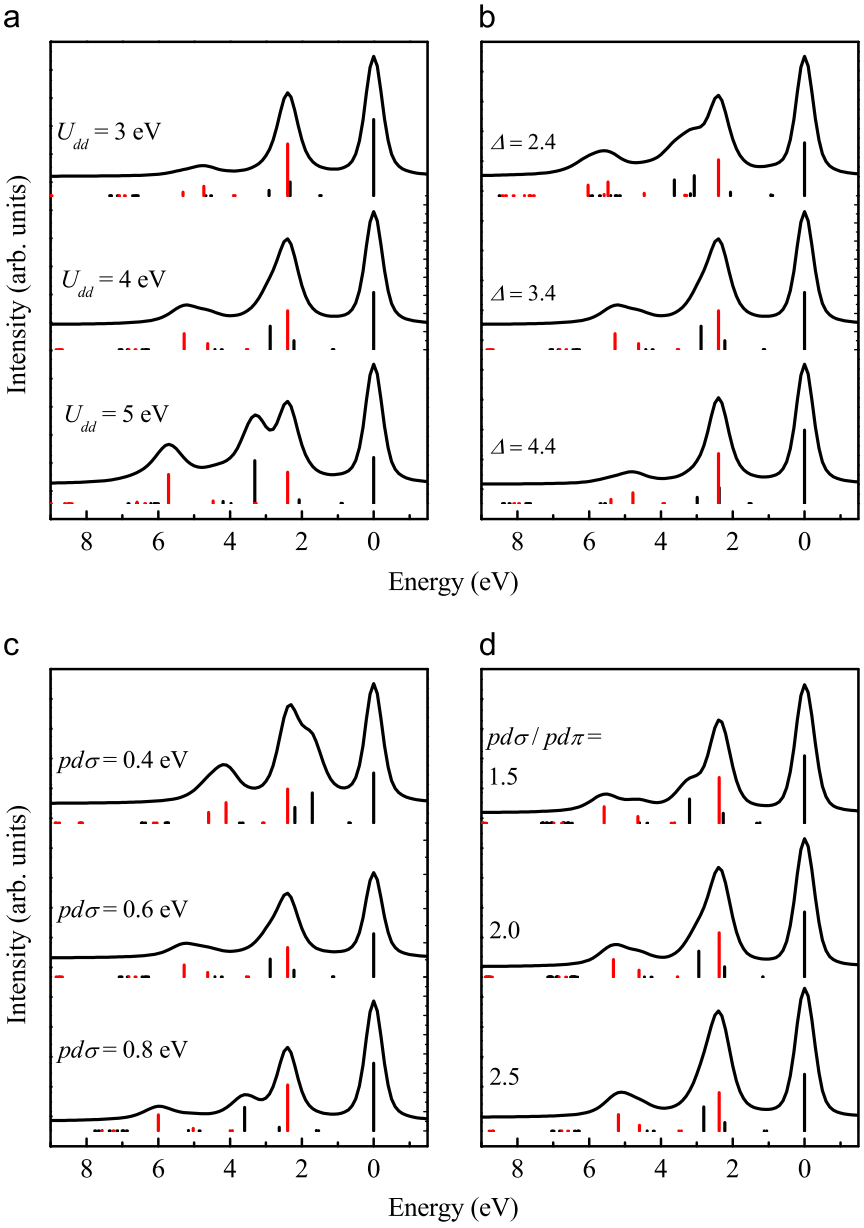

Fig. 3. Calculated 3*d* spectrum as a function of (a) U_{dd}, (b) Δ, (c) $pd\sigma$ and (d) ratio, $pd\sigma/pd\pi$ keeping the other parameters unchanged. These results establish reliability of the parameter values.

keeping other parameters unchanged. It is evident that the change in parameter values exhibit significantly different spectral functions. The increase in U_{dd} and $pd\sigma$ leads to an increase in energy separation between the main peak and the satellite, while the increase in Δ reduces the energy separation. The relative intensity of the main peak and the satellite evolves differently for the change in U_{dd} and Δ. The change in $pd\sigma$ leads to significant change in relative intensities of different satellite features – the feature 3 becomes stronger than feature 2 with the increase in $pd\sigma$. An increase in the ratio, $pd\sigma/pd\pi$, leads to a decrease in the main peak-satellite energy separation. These results demonstrate that the calculated spectral function is quite sensitive to the parameter values.

In order to investigate the reliability of these estimations further, we have simulated a completely different spectral function, namely the Zr 3*p* spectrum within the same model and parameter set. The calculated results for the parameters corresponding to the fit in Fig. 2(b) are shown in Fig. 4. Evidently, the representation of the experimental spectrum is outstanding. The main peak denoted by '1' in the final state spectrum corresponds to 22.39%, 32.58%, 27.14%, 13.91%, and 3.95% while the satellite peak, marked 2 in the figure, possesses 72.11%, 4.87%, 1.08%, 17.36%, and 4.55% contributions from $|d^2\rangle$, $|d^3L^1\rangle$, $|d^4L^2\rangle$, $|d^5L^3\rangle$ and $|d^6L^4\rangle$ configurations, respectively. In the satellite peak, the dominant contribution arises from the $|d^2\rangle$ character while the $|d^3L^1\rangle$ state contributes primarily to the main peak along with significant contributions from $|d^2\rangle$ and $|d^4L^2\rangle$ states as expected for such photoemission signals.

4. Discussion

The 4*d* transition metals possess large radial extension of the 4*d* orbitals. Thus, the electron–electron Coulomb repulsion

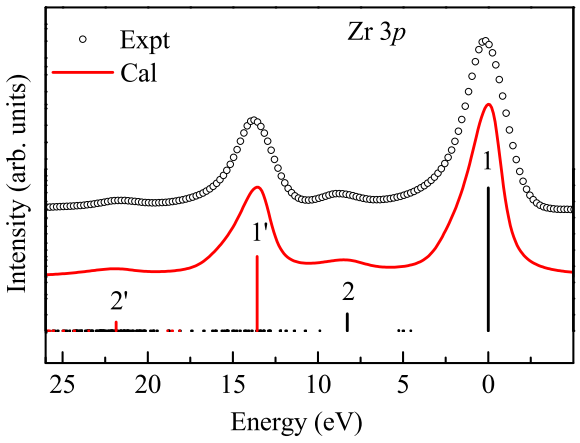

Fig. 4. Calculated Zr 3*p* spectrum for the parameter values corresponding to the Zr 3*d* spectrum shown in Fig. 2(b). Symbol shows the experimental spectrum, line represents the calculated broadened spectrum and bars are the energies with corresponding intensities. '1' and '2' denote the main peak and satellite of the $3p_{3/2}$ signal. The primed numbered features correspond to the spin–orbit split features.

strength in these systems is expected to be relatively weaker than that in 3*d* transition metal based systems. Moreover, the large size of the B_{12} units in ZrB_{12} is expected to provide huge void space for the Zr sites with significant freedom for Zr-movements [21,22] – the coupling of the Zr-vibrations with the electronic structure is expected to be strong. Such scenario prompted the justification for the observation of conventional superconductivity in this compound, where the electron–electron pairing can easily be explained on the basis of electron–phonon coupling [1–3]. However, significant conflicting observations in the electronic properties generated puzzles in this system.

Here, we observe a significantly large U_{dd} value (~4 eV). While this seems unusual, such behavior has been observed earlier in other 4*d* and 5*d* transition metal based compounds, in particular oxides [18–20]. The magnitude of U_{dd} in ZrB_{12} is quite similar to the estimated values of U_{dd} in 3*d* transition metal oxides. This suggests that the change in radial extension of the *d* orbitals does not have significant influence in the electronic structure of these complex compounds – presumably there are other competing factors not realized so far. One possibility could be the vibrations of the Zr atoms within the huge void space that introduces uncertainty in the Zr position. Hence, the hopping interactions would significantly be affected leading to a greater degree of electron localization. This is manifested in the magnitude of $pd\sigma$ being 0.6 eV – somewhat smaller than the typical values found in 3*d* transition metal based systems. The other factor is the absence of B atoms on the Zr–Zr axis despite the fact that a large number of borons are present in each crystalline unit. This would make the $pd\sigma$ value smaller. Thus, the electron localization in these systems is quite strong due to the reduced degree of electron hopping to the next sites albeit large radial extension of the 4*d* orbitals.

In addition, the value of U_{dd} describing the electronic spectra of ZrB_{12} is found to be larger than the charge transfer energy, which places this compound in the charge transfer regime of the modified ZSA phase diagram [16]. Such a characterization of an early 4*d* transition metal system (the first group of the transition metal series in the periodic table) is unusual and in sharp contrast to the scenario in early 3*d* transition metal series exhibiting Mott–Hubbard-type behavior. The electronic band structure calculations [10] exhibit a large bandwidth of the B 2*p* bands and the valence band is primarily constituted by the B 2*p* contributions. Such a scenario appears due to the large B_{12} size leading to strong hybridization among the B 2*p* orbitals. This could be one possible reason for the reduction in the energy difference between the *d* and *p* levels making a smaller charge transfer energy. Clearly, more studies are necessary to find the origin of such anomalous behavior.

5. Conclusion

In conclusion, we studied the core level spectra of ZrB_{12} using configuration interaction within a $Zr(B_{12})_6$ cluster and the multi-band Hubbard model. This model has been found to be successful in 3*d* transition metal systems. Here, we show that the scenario is quite similar in the case of 4*d* transition metal based compounds too. The parameterized model calculations provide a remarkably good representation of the experimental spectra – the same set of parameters could produce both 3*d* and 3*p* spectra well. The electron correlation strength is found to be significant that might be responsible for the complexity in the electronic properties in an otherwise simple system. Interestingly, the charge transfer energy is found to be smaller than the on-site correlation strength putting these materials in the charge transfer regime in contrast to the cases of early 3*d* transition metal systems.

Appendix A. Supplementary data

Supplementary data associated with this article can be found in the online version at http://dx.doi.org/10.1016/j.ssc.2014.05.027.

References

[1] A.V. Rybina, K.S. Nemkovski, P.A. Alekseev, J.-M. Mignot, E.S. Clementyev, M. Johnson, L. Capogna, A.V. Dukhnenko, A.B. Lyashenko, V.B. Filippov, Phys. Rev. B 82 (2010) 024302.
[2] J. Teyssier, R. Lortz, A. Petrovic, D. van der Marel, V. Filippov, N. Shitsevalova, Phys. Rev. B 78 (2008) 134504.
[3] Y. Wang, R. Lortz, Y. Paderno, V. Filippov, S. Abe, U. Tutsch, A. Junod, Phys. Rev. B 72 (2005) 024548.
[4] Daghero, R.S. Gonnelli, G.A. Ummarino, A. Calzolari, V. Dellarocca, V.A. Stepanov, V.B. Filippove, Y.B. Paderno, Supercond. Sci. Technol. 17 (2004) S250.
[5] V.A. Gasparov, N.S. Sidorov, I.I. Zver'kova, Phys. Rev. B 73 (2006) 094510.
[6] D.P. Young, et al., Nature 397 (1999) 412;
P. Vonlanthen, et al., Phys. Rev. B 62 (2000) 10076;
K. Maiti, V.R.R. Medicherla, S. Patil, R.S. Singh, Phys. Rev. Lett. 99 (2007) 266401;
K. Maiti, Europhys. Lett. 82 (2008) 67006.
[7] H. Werheit, V. Fillipov, K. Shirai, H. Dekura, N. Shitsevalova, U. Schwarz, M. Armbruster, J. Phys.: Condens. Matter 23 (2011) 065403.
[8] B.T. Matthias, T.H. Geballe, K. Andres, E. Corenzwit, G.W. Hull, J.P. Maita, Science 159 (1968) 530.
[9] S. Thakur, D. Biswas, N. Sahadev, P.K. Biswas, G. Balakrishnan, K. Maiti, J. Appl. Phys. 114 (2013) 053904.
[10] S. Thakur, D. Biswas, N. Sahadev, P.K. Biswas, G. Balakrishnan, K. Maiti, Sci. Rep. 3 (2013) 3342.
[11] K. Maiti, P. Mahadevan, D.D. Sarma, Phys. Rev. B 59 (1999) 12457;
K. Maiti, D.D. Sarma, Phys. Rev. B 54 (1996) 7816;
K. Maiti, D.D. Sarma, T. Mizokawa, A. Fujimori, Europhys. Lett. 37 (1997) 359.
[12] K. Okada, A. Kotani, J. Phys. Soc. Jpn. 61 (1992) 4619;
K. Okada, A. Kotani, K. Maiti, D.D. Sarma, J. Phys. Soc. Jpn. 65 (1996) 1844.
[13] A.E. Bocquet, T. Mizokawa, T. Saitoh, H. Namatame, A. Fujimori, Phys. Rev. B 46 (1992) 3771;
A.E. Bocquet, T. Mizokawa, K. Morikawa, A. Fujimori, S.R. Barman, K. Maiti, D. D. Sarma, Y. Tokura, M. Onoda, Phys. Rev. B 53 (1996) 1161.
[14] D.D. Sarma, Phys. Rev. B 37 (1988) 7948;
D.D. Sarma, S.G. Ovchinnikov, Phys. Rev. B 42 (1990) 6817;
D.D. Sarma, J. Phys. Soc. Jpn. 65 (1996) 1325.
[15] A. Fujimori, F. Minami, Phys. Rev. B 30 (1984) 957;
A. Fujimori, N. Kimizuka, T. Akahane, T. Chiba, S. Kimura, F. Minami, K. Siratori, M. Taniguchi, S. Ogawa, S. Suga, Phys. Rev. B 42 (1990) 7580.
[16] D.D. Sarma, H.R. Krishnamurthy, Seva Nimkar, S. Ramasesha, P.P. Mitra, T.V. Ramakrishnan, Pramana (J. Phys.) 38 (1992) L531.
[17] J. Zaanen, G.A. Sawatzky, J.W. Allen, Phys. Rev. Lett. 55 (1985) 418;
J. Zaanen, C. Westra, G.A. Sawatzky, Phys. Rev. B 33 (1986) 8060.
[18] R.S. Singh, V.R.R. Medicherla, K. Maiti, E.V. Sampathkumaran, Phys. Rev. B 77 (2008) 201102(R);
K. Maiti, Solid State Commun. 149 (2009) 1351;
R.S. Singh, K. Maiti, Phys. Rev. B 76 (2007) 085102;

K. Maiti, R.S. Singh, Phys. Rev. B 71 (2005) 161102(R);
K. Maiti, R.S. Singh, ScienceJet 3 (2014) 55.
[19] M. Takizawa, D. Toyota, H. Wadati, A. Chikamatsu, H. Kumigashira, A. Fujimori, M. Oshima, Z. Fang, M. Lippmaa, M. Kawasaki, H. Koinuma, Phys. Rev. B. 72 (2005) 060404.
[20] B.J. Kim, H. Jin, S.J. Moon, J.-Y. Kim, B.-G. Park, C.S. Leem, J. Yu, T.W. Noh, C. Kim, S.-J. Oh, J.-H. Park, V. Durairaj, G. Cao, E. Rotenberg, Phys. Rev. Lett. 101 (2008) 076402.
[21] B. Post, F.W. Glaser, J. Metals Trans. AIME 631 (1952).
[22] Yu. B. Paderno, A.B. Liashchenko, V.B. Filippov, A.V. Dukhnenko, in: V.V. Skorokhod (Ed.), Advantages and Challenges in Science for Materials in the Frontier of Centuries, IPMS, Kiev, 2002, p. 347.
[23] Z. Fisk, B.T. Matthias, Science 165 (1969) 279.
[24] J.C. Slater, G.F. Koster, Phys. Rev. 94 (1954) 1498.
[25] D. van der Marel, G.A. Sawatzky, Phys. Rev. B 37 (1988) 10674.